Linearized Tropopause Dynamics and Cyclone Development

RICHARD GROTJAHN

National Center for Atmospheric Research,[1] Boulder, CO 80307

(Manuscript received 21 April 1980, in final form 14 August 1980)

ABSTRACT

A preliminary investigation into the dynamical effects produced by the tropopause upon a midlatitude wave cyclone is described. This article describes linear effects since the various structures of a *fixed* tropopause are examined. In general, the solutions are sensitive to changes in tropopause structure only when they have large amplitude in the tropopause vicinity or the forcing for the problem is significantly altered by the tropopause structure. The forcing is greatest at the bottom boundary and interior tropopause interface. The basic current contains an internal jet. Many characteristic properties of this jet were found in a less sophisticated antecedent study where the velocity maximum occurred at the top boundary. This research forms the basis for future inquiry into nonlinear tropopause dynamics.

1. Exordium

This article presents the inaugural results of my research into how the structure and dynamics of the tropopause modify and interact with the incipient development of a midlatitude traveling wave cyclone. For convenience, I refer to the area of investigation that encompasses this problem as tropopause dynamics. Yet, this study will focus upon the properties of the wavelike solutions of a simple mathematical model. In this report only the linearized aspects of tropopause dynamics are examined; future work will consider some nonlinear effects.

This study employs a model that examines the properties of incipient eddies growing within a prescribed mean flow field. The prescribed thermodynamic properties of the fluid typify those properties of the troposphere in the lower portion of the domain and the stratosphere in the upper part. In between is a transition zone which is arbitrarily designated the tropopause region. In the experiments, this zone can be broad, narrow, infinitesimally thin, or tilted in the meridional dimension. A meridionally uniform zonal velocity field that reaches a maximum near the mid-height of the tropopause zone is considered first. Two other zonal flows are examined which have an internal jet superimposed on that meridionally uniform flow. In one case, the jet is associated with a weak thermal front strongest at the lower surface; in the other case, the weak front is strongest near the tropopause level. For convenience, the label "front" is used in this article to refer to a region where the meridional gradient of the prescribed temperature field reaches a maximum. This study is neither intended nor capable of specifically examining the stronger, narrower fronts observed in the earth's atmosphere.

There are some previous investigations of how the vertical structure of static stability affects cyclone-scale waves. Moen (1974) found that the maximum growth rate occurred at shorter wavelengths when the static stability was reduced in the lower levels of his model. This result was supported by Duncan (1977) using observed data in a study of polar lows. Staley and Gall (1977) showed that the stability and structure of solutions for a four-level model were responsive to various profiles of static stability and also vertical shear in the mean state. The short waves were especially sensitive to the mean state profiles. In a study of mid-ocean eddies, Gill *et al.* (1974) deduced that seasonal changes in the upper few hundred meters of the velocity and density profiles could significantly alter the growth rates and structures of the modes. The near-surface trapped modes seemed particularly affected. Simmons and Hoskins (1977) found that including a more realistic mean-state tropopause (with the low-level mean fluid unchanged) had little effect on the low-level structure of their solutions. However, for intermediate-length waves, the upper level amplitude was increased. Blumen (1979) considered the role of the relative depths of two layers of differing static stability.

This study also shows that different tropopause structures generally create modest linearized changes in the solutions. The effects are more pronounced

[1] The National Center for Atmospheric Research is sponsored by the National Science Foundation.

0022-4928/80/112396-11$06.75

for solutions with relatively large amplitude in the tropopause region. These are the long and some intermediate scale waves, as well as solutions for the case where the thermal front occurs principally in the tropopause zone. The alterations of the other solutions are insignificant.

One premise for this investigation of tropopause dynamics is that adequate resolution of the narrow atmospheric tropopause will significantly improve the numerical forecasts of observed wave-cyclones. While the spatial resolution does not appear to be critical for weakly unstable flows (Bleck, 1979), it may be important in cases where the meridional temperature gradient is much stronger. The theoretical aspects of this question are not adequately considered using the present series of experiments; instead, these experiments provide a foundation for future examination of this and related questions.

2. Model description

The mathematical model used in these experiments is patterned after that delineated in Grotjahn (1979). The details of its derivation can be found in that reference. The current model incorporates several improvements on the earlier version and these differences will be emphasized in this section.

This analysis is restricted to the quasi-geostrophic equations expressed on a midlatitude β-plane. A potential vorticity equation constrains the fluid motion in the interior of a zonally oriented channel. The boundary conditions are periodic in x, and vanishing normal velocity along the y and z boundaries. (A list of symbols is presented in the Appendix.)

A rigid lid is an undesirable boundary condition for this model if it importantly affects the solution. Such was the case in Grotjahn (1979) where the lid was placed at 10 km in order to crudely represent the tropopause. Following the analysis of Charney and Drazin (1961), the real part of the "refractive index" for the lowest-order potential vorticity equation is negative above 20 km or less, for all wavelengths. In these experiments, the upper lid is placed at 50 km. Hence this upper boundary condition is now more reasonable because the vertical propagation of energy at the top is negligible. Indeed, a solution is virtually unchanged for any top boundary position above 25 km.

The equations are nondimensionalized about a static state whose properties are chosen to fit the typical midlatitude horizontal mean structure of the earth's atmosphere. Unlike Grotjahn (1979), a deep upper region of the fluid representing the stratosphere is now included. The equations are linearized about a basic state $\psi(y,z)$. Eddy solutions $\phi(x,y,z,t)$ are sought that are assumed to be small. Therefore, only the incipient stages of cyclone development can be treated with this model and the eddy does not modify the basic state.

Asymptotic series solutions are sought to the equations. The y, z structure $\hat{\phi}$ and complex phase speed C of the wave solutions are expanded in powers of the small Rossby number μ. The basic state is also expanded in order to make the equations separable. This restriction is no longer required, because all the results are calculated by numerical methods. However, it does allow greater resolution and celerity in the calculations.

One must solve a complex, two-dimensional, possibly singular Poisson equation at each order in μ. At lowest order the interior and boundary equations are homogeneous. In Grotjahn (1979), the lowest-order, basic-state potential vorticity gradient $\bar{q}_{0y}$ is zero everywhere in the interior [see Eqs. (2a) and (4a)]. This constraint is now removed, allowing quite general profiles of mean zonal velocity, static stability, etc. By inspection of (2a), the lowest-order equations compose a *generalized* eigenvalue problem for the eigenvalue C_0. The derivatives are approximated by finite differences in y and z. The resulting system of linear equations constitutes a matrix generalized eigenvalue problem that is solved utilizing a highly accurate numerical routine. At higher orders the equations are generally heterogeneous and solved in the following manner. Since the same differential operator appears on the left-hand sides of Eqs. (2) at each order, their forcing functions must satisfy an orthogonality condition in order to obtain a solution. This condition specifies the higher-order terms in the complex phase speed series (i.e., C_i for $i > 0$). The structure is determined using a fast direct numerical technique to solve the Poisson equation. See Grotjahn (1979) for more details about how the higher-order solutions are obtained.

The fluid in these experiments extends from the bottom surface ($z = 0$) to 50 km ($z = 5$). The mid-height of the tropopause zone is placed at 10 km. Since we are primarily interested in the results below 15–20 km the coordinate transformation

$$\xi = 1 - \exp(-z) \tag{1}$$

is employed. This transform provides high resolution in the bottom portion of the domain and coarse resolution in the top region. Typically, the number of levels utilized in the calculations was 50 or 75. This resolution seems altogether adequate since trial calculations using 25 levels were hardly distinguishable for most wavelengths.

The interior equation can be written

$$\mathcal{L}(\hat{\phi}_i) \equiv (U_0 - C_0)\{\epsilon\hat{\phi}_{izz} + (\Omega\epsilon + \epsilon_z)\hat{\phi}_{iz} + \hat{\phi}_{iyy} - k^2\hat{\phi}_i\} + \bar{q}_{0y}\hat{\phi}_i = F_i, \tag{2a}$$

where a wavelike dependence on x and t has been

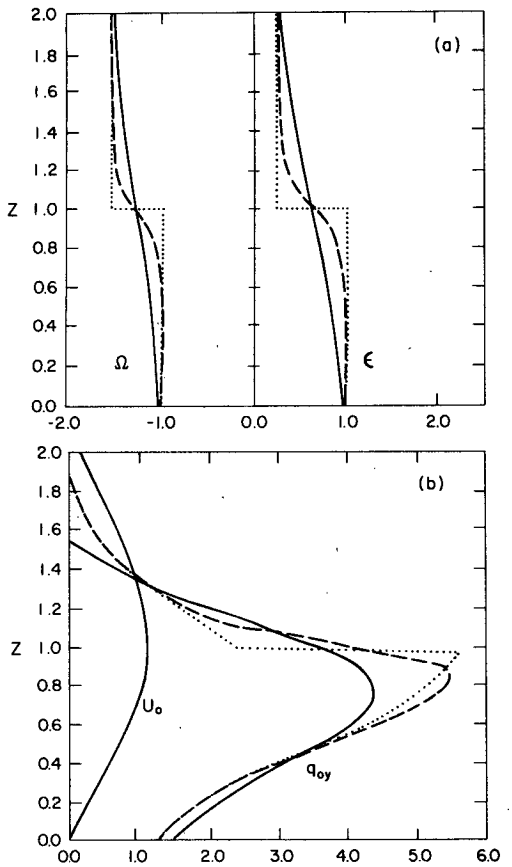

FIG. 1. Vertical profiles of a) ϵ and Ω and b) U_0 and $\bar{q}_{0y}$ for the Broad (solid line), Narrow (dashed line) and Interface (dotted line) cases. U_0 is the same in all cases.

assumed:

$$\phi_i = \hat{\phi}_i(y,z) \exp[ik(x - Ct)]. \tag{3}$$

The subscripts refer either to differentiation or the order in the Rossby number expansion. The meridional gradient of basic-state potential vorticity is written

$$\bar{q}_{0y} = \beta - \epsilon U_{0zz} - (\Omega\epsilon + \epsilon_z)U_{0z}. \tag{4a}$$

The periodic x boundary conditions are automatically satisfied by (3). The other boundary conditions are

$$\hat{\phi}_i = 0 \quad \text{along} \quad y = \pm y_b, \tag{2b}$$

where y_b equals one-quarter of the x wavelength, and

$$\mathcal{D}(\hat{\phi}_i) \equiv (U_0 - C_0)\hat{\phi}_{iz} - U_{0z}\hat{\phi}_i = B_i$$

at

$$z = 0, 5. \tag{2c}$$

At lowest order $F_0 = B_0 = 0$. The orthogonality condition prescribing C_1 is given by (9) in Section 4. The lowest order solution is discussed next.

For the lowest-order problem there are as many eigensolutions as there are grid points in the vertical for any given set of parameters. However, we are interested in only one of these solutions. For the intermediate waves there is usually only one solution with a large growth rate, the other solutions are neutral or nearly so. For most wavenumbers it is sufficient to select the proper solution by choosing the fastest growing mode. A partial check is made by performing the operation with a much different resolution and requiring the two selected eigenvalues to be almost the same. This procedure accurately reproduces the results in Green (1960) and the analytic solution in Árnason *et al.* (1967). However, it is not always appropriate when the desired solution is neutral or nearly so, as will be shown in Grotjahn (1981). Árnason *et al.* (1967) show that when the true solution is neutral, the finite difference approach may not converge to the correct result because the finite differencing improperly handles singularities in the equations. This report will focus on rapidly growing solutions for which this convergence problem is not encountered. Finally, the higher-order solutions are uniquely dependent on the lowest-order solution.

3. First-order solutions

In this section the lowest order solution ($i = 0$) to the generalized eigenvalue problem (2) is examined. Three profiles of static stability (and correlative profiles of Ω) are considered. The values of the static stability κ, at the top and bottom boundaries, approximate those calculated from the U.S. Standard Atmosphere. We let ϵ nearly equal 1 at the lower surface (in order to define the horizontal length scale L) and allow it to vary in accordance with κ. The following mathematical expression is used:

$$\epsilon \equiv \frac{f_0^2 L^2}{g\kappa D} = 0.70 - 0.35 \tanh[\lambda(z - z_T)], \tag{4b}$$

where z_T is the mid-height of the tropopause and λ is inversely related to the depth of the tropopause zone. Two of the experiments are for $\lambda = 1$ and $\lambda = 5$; they are labeled the Broad and Narrow cases, respectively. The third experiment comprises an infinitesimally thin interface between upper and lower fluids, each with constant κ, ϵ and Ω, and is referred to as the Interface case. These three cases are diagramed in Fig. 1.

In the Interface case two additional conditions are applied at the interface ($z = z_T$):

$$\phi_i^u = \phi_i^L, \tag{5a}$$

the dynamic condition, and

$$\epsilon^u[\phi_{iz}^u(U_0 - C_0) - U_{0z}\phi_i^u] = \epsilon^L[\phi_{iz}^L(U_0 - C_0) - U_{0z}\phi_i^L], \tag{5b}$$

the kinematic condition. The superscripts refer to variables evaluated in the upper (u) or lower (L) fluid. These conditions express continuity of pressure and normal velocity across the interface.

In the atmosphere, the mean zonal flow often reaches a maximum near the tropopause level. In the winter hemisphere there is often a stronger jet at much higher altitude; but the zonal winds at the tropopause may still be a relative maximum. To model this observed structure, the lowest order basic state velocity is defined

$$U_0 = 1.8[1.0 - \tanh^2(z - z_T) - \omega \exp(-0.1z)], \quad (6)$$

where $\omega = 1.0 - \tanh^2(z_T)$. This profile reaches a maximum near z_T, vanishes at $z = 0, \infty$, and is only a function of height. It is plotted in Fig. 1 along with $\bar{q}_{0y}$.

All coefficients in the model at lowest order are independent of y. Thus, the y dependence of ϕ_0 can be specified and $\cos(ky)$ is chosen. This choice satisfies (2b).

Phase speed spectra for the experiments are portrayed in Fig. 2. For the long ($\alpha < 1.1$) and short waves ($\alpha > 2.5$), the phase speed decreases with wavelength. For most intermediate waves it is nearly constant or increases with decreasing wavelength. As the tropopause zone becomes sharper, the intermediate and short waves propagate faster. Near $\alpha = 1.1$ is a cusp separating the long and intermediate wavelength solutions; much like that found in earlier studies of this kind.

The growth rate spectra are also shown in Fig. 2. The most unstable wavelength is around 4500 km ($\alpha = 2.0$). As for the propagation speed, the growth rate spectra for the Narrow and Interface cases are very similar. There is generally a trend between the three cases as one might expect. A fourth case is included in Fig. 2 wherein the rigid lid is placed at z_T. This low rigid lid greatly reduces the long-wave growth rates, a result evident in previous studies. The long and intermediate waves propagate slower. The low lid hardly modifies the short waves.

Vertical profiles of the amplitude and phase are plotted in Fig. 3. The solution for $\alpha = 0.8$ is representative of the long-wave solutions; that for $\alpha = 2.0$ represents the intermediate waves; that for $\alpha = 3.0$ typifies the short waves. The differences between the three cases are small, but most apparent for the long waves. The height of the long-wave upper maximum in amplitude is increased as the tropopause zone is thinned. If the "stratosphere" is removed and a rigid lid is placed at z_T then the upper tropospheric amplitude is significantly increased. The layer of rapid phase shift is shallower for a broader tropopause. (Phase angle decreasing with increasing height implies westward tilt with height.) This indicates that the mid-tropospheric westward tilt with height of the pressure trough and ridge axes

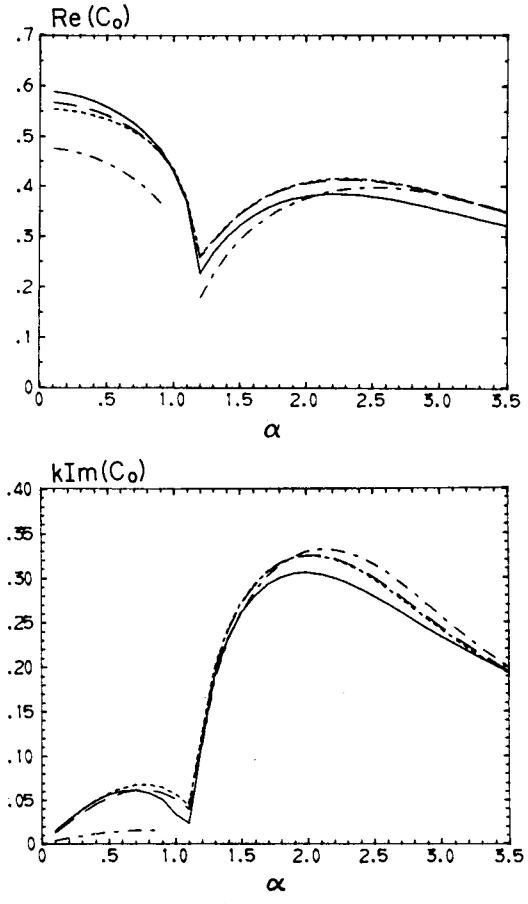

FIG. 2. Lowest-order phase speed and growth rate spectra for the cases: Broad (solid line), Narrow (dashed line), Interface (dotted line) and Narrow with upper boundary at $z = 1$ (dot-dashed line). α is proportional to wavenumber.

is stronger for the more diffuse tropopause. The intermediate-wave solutions vary between the three cases to a lesser extent. The short waves are effectively bottom trapped; so the differences between the three cases are insignificant. Notice the kink in the $|\phi_0|$ profiles for the Interface case brought about by the discontinuity in κ at z_T. This suggests a *possible* discontinuity in the eddy potential temperature. This is not certain because the potential temperature can be related to pressure and its vertical derivative through an equation incorporating κ so the discontinuities may be compensating.

4. Second-order solutions

Consideration is now given to two mean zonal flows containing horizontal and vertical shear associated with a weak thermal "front." It is important to note that true atmospheric fronts are stronger, narrower and not properly handled by this model.

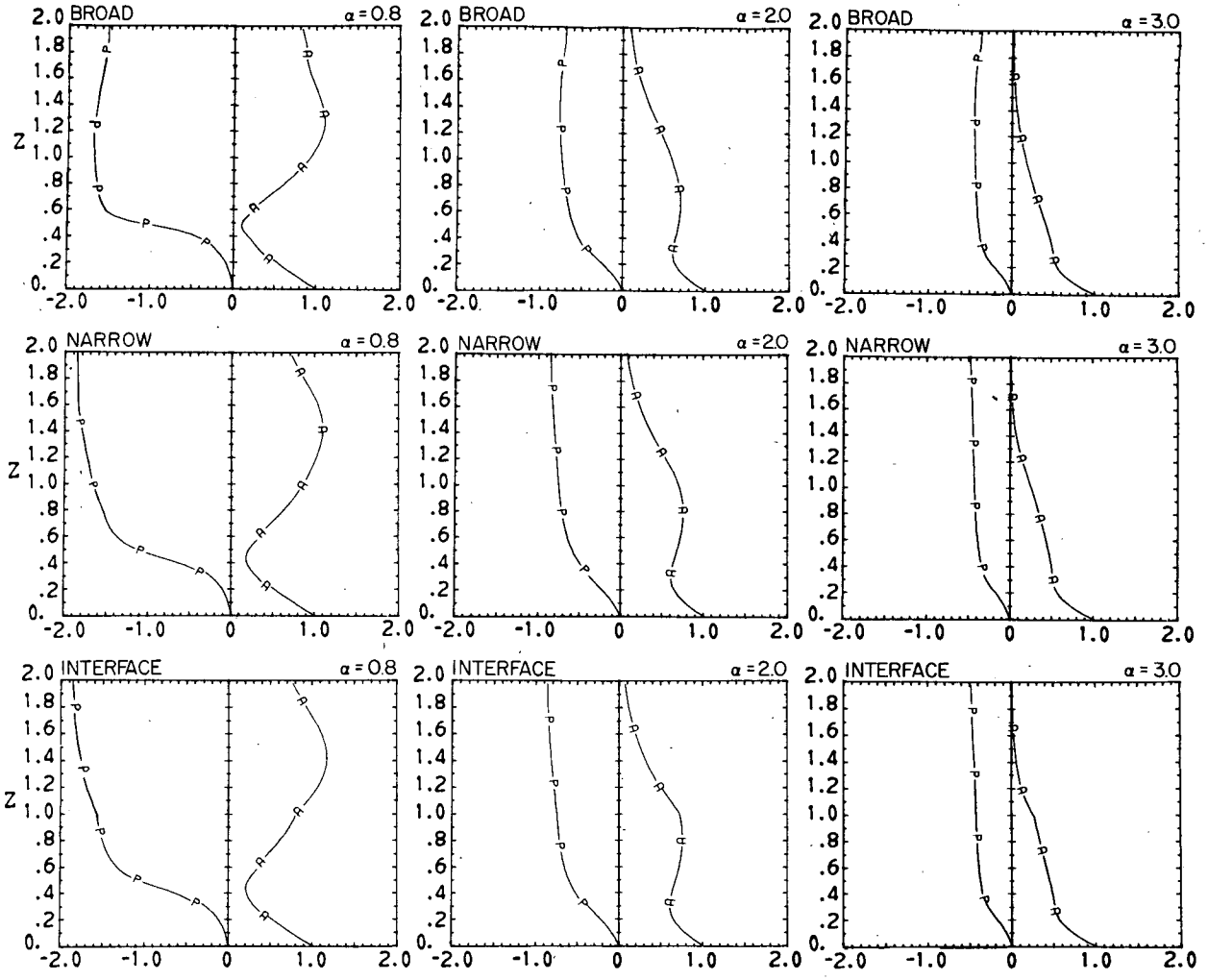

FIG. 3. Vertical profiles of lowest-order pressure amplitude (A) and one-half phase angle (P) for the Broad, Narrow and Interface cases. The profiles for $\alpha = 0.8$, 2.0 and 3.0 are representative of the long, middle and short waves, respectively.

Neglecting the small exponential factors that control their high-altitude amplitude, two similar mean-state prescriptions were analyzed previously in Grotjahn (1979). Discussion is also presented of a case where the tropopause zone has a meridional tilt, higher toward the equator. Yet, the two cases where an internal jet occurs in the mean flow will receive our primary attention.

The second-order interior equation forcing function is given by

$$F_1 = \hat{\phi}_0\left[\bar{q}_{0y}\left(\frac{U_1 - C_1}{U_0 - C_0}\right) - \bar{q}_{1y}\right], \quad (7a)$$

where $\bar{q}_{0y}$ is defined by (4), $U_1 = -\psi_{1y}$, and

$$\bar{q}_{1y} = -U_{1yy} - \epsilon U_{1zz} - (\Omega\epsilon + \epsilon_z)U_{1z}. \quad (8)$$

The second-order vertical boundary conditions are heterogeneous with

$$B_1 = (C_1 - U_1)\hat{\phi}_{0z} + U_{1z}\hat{\phi}_0. \quad (7b)$$

The second-order orthogonality condition can be expressed as a definition for C_1:

$$C_1 = \frac{\iint \frac{\rho_s\hat{\phi}_0^2}{U_0 - C_0}\left[\frac{U_1\bar{q}_{0y}}{U_0 - C_0} - \bar{q}_{1y}\right]dydz + \int \epsilon\rho_s\hat{\phi}_0\left[\frac{U_1U_{0z}\hat{\phi}_0}{(U_0 - C_0)^2} - \frac{U_{1z}\hat{\phi}_0}{U_0 - C_0}\right]\Bigg|_{z=0}^{z=5}dy}{\iint \frac{\phi_0^2\rho_s\bar{q}_{0y}}{(U_0 - C_0)^2}dydz + \int \frac{\epsilon\rho_s\phi_0^2U_{0z}}{(U_0 - C_0)^2}\Bigg|_{z=0}^{z=5}dy}. \quad (9)$$

The meridional structure of each weak thermal front is the same, i.e.,

$$\left.\begin{aligned}\psi_1 &= -G(z)[\lambda \tanh(ay) - b_1 y - b_2 y^3] \\ U_1 &= G(z)[a\lambda[1 - \tanh^2(ay)] - b_1 - 3b_2 y^2]\end{aligned}\right\}. \quad (10a)$$

This meridional structure is discussed in Grotjahn (1979). As before, $\lambda = 2.0/\tanh(2.25a)$, $y_b \approx 2.2$ for $\alpha = 1.0$, $b_1 = 1.1$ and $b_2 = 0.03$. The intensity and meridional width of the frontal zone can be altered systematically by varying the parameter a. As a increases the intensity increases and the width decreases by adiabatic compression of the isotherms. The two fronts are distinguished by their vertical structure:

$$\left.\begin{aligned}G(z) &= (2z - z^2)\exp(-0.1z)\Lambda \\ &\qquad\qquad \text{(surface front case)} \\ G(z) &= (z^2 - (5/12)z^3)\exp(-0.2z)\Lambda \\ &\qquad\qquad \text{(upper front case)}\end{aligned}\right\}. \quad (10b)$$

In the surface front case, the thermal front is most intense at $z = 0$, the bottom surface; in the upper front case it is strongest at $z = 0.8$. The parameter Λ is used to control the basic state available potential energy ($\overline{\text{APE}}$). In Table 1, values of Λ are listed that make the $\overline{\text{APE}}$ equivalent for all cases. In some of the following discussion the $\overline{\text{APE}}$ is fixed and these values of Λ have been used; in other instances it seemed more useful to examine identical basic velocity fields with different $\overline{\text{APE}}$.

An attempt was made to model the observed meridional slope of the tropopause. The tilt of the tropopause implies y variation of the basic state static stability. This variation introduces an additional zonal velocity field which is modeled by defining

$$U_T = -2(y + \Delta)\Upsilon \tanh(z - z_T)U_0, \quad (11)$$

where Υ is proportional to the degree of tilt. This choice of U_T is made so that the y and z dependences are separable. This $O(\mu)$ portion of the basic-state current can be handled independently of the flow associated with the front. Fig. 4 shows an example of an upper front basic state that includes the tropopause tilt specified by (11).

Fig. 5 shows second-order phase speed spectra for the three cases with the upper front. The phase speed of the long waves is decreased by the front;

TABLE 1. Values of Λ for equivalent $\overline{\text{APE}}$.

	Broad case	Narrow case	Interface case
Surface front	1.0366	1.	0.9998
Upper front	3.0151	2.2117	2.1915

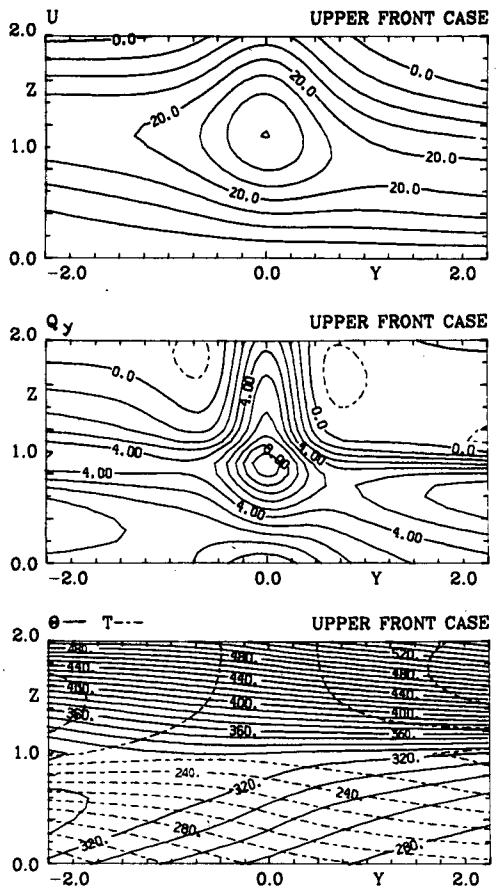

FIG. 4. Meridional cross sections of the prescribed fields of zonal velocity $U = U_0 + \mu(U_1 + U_T)$, potential vorticity gradient $\bar{q}_y$, temperature T and potential temperature Θ, for the upper front Narrow case including tropopause tilt, where $\Lambda = 2.2117$, $\Upsilon = 1.0$ and $\Delta = 0$. The units are m s^{-1} and K; $\bar{q}_y$ is nondimensional.

the other waves propagate faster. The shorter wave speeds are increased the most. Since a lowest order phase speed maximum exists near $\alpha = 2.3$, it is clear that the front shifts the fastest moving wave to shorter wavelengths. Consistent comments can be made for the surface front experiments, with the shift being even greater (see Fig. 7). The complex phase speed of the middle and short waves is noticeably affected by the tropopause structure only in the upper front cases; hence the surface front results will be only briefly described. If the $\overline{\text{APE}}$ is made equivalent for each of the tropopause structures, the broad tropopause allows faster propagation of the solutions. When the basic velocity fields are the same (as they are in Fig. 5), then the Interface and Broad tropopause results are nearly identical and the Narrow case solutions propagate faster.

The second-order growth rates for the upper front experiments are exhibited in Fig. 6. Nearly all the waves grow faster. Since the lowest order growth

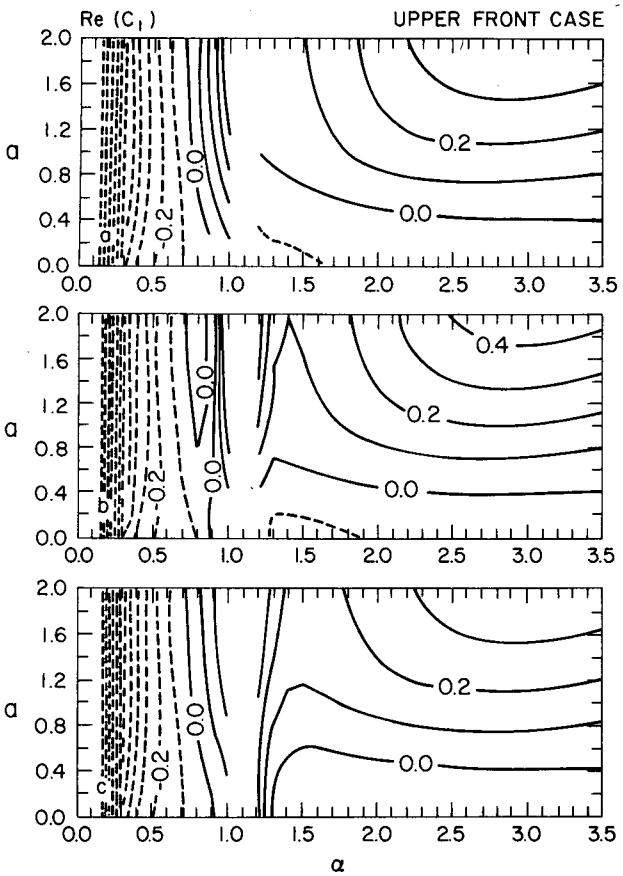

FIG. 5. Second-order phase speed spectra for the upper front a) Broad, b) Narrow and c) Interface cases. As a increases, the thermal front intensity increases and its meridional scale decreases. The contour interval is 0.1; dashed contours indicate negative values in Figs. 5–9. $\Lambda = 2.2117$ in all cases. The blank regions in Figs. 5, 6, 7 and 9 are centered about $\alpha = 1.1$ where Eq. (9) is singular.

rate maxima occurred near $\alpha = 2.0$, the thermal front causes a shift of the most unstable wavelength to shorter waves. This shift is much larger for the surface front experiments once again. When the $\overline{APE}$ is kept fixed, the growth rates are almost the same, as might be expected, though the Broad case solutions are more efficient at converting available potential energy.

The total growth rate and phase speed spectra for the surface front Interface case are shown in Fig. 7. The corresponding spectra for the upper front Interface case also appear in this figure. ("Total" refers to truncating the asymptotic series after summing the first two terms.) This figure may be compared with Fig. 14 in Grotjahn (1979). The models used for each calculation are the same below the interface, except that there is now a nonvanishing interior $\bar{q}_{0y}$. More specifically, the lowest-order vertical shear U_{0z} is now large in the middle and lower troposphere and very small near z_T—the opposite of before. That distribution of vertical shear and the low rigid lid at $z = 1$, caused the earlier solutions to have much greater amplitude at z_T than the current results. These differences account for the vicissitudinous phase speed spectra (the middle waves were slowed down before). Despite these differences, the same most unstable wavelength shift was seen in the antecedent study. An analogous shift can be found in the results of Brown (1969, Fig. 2) and Song (1971). To facilitate the comparison, note that as a increases the kinetic and available potential energies of the mean flow increase geometrically (the kinetic at a faster rate). Also, these solutions are principally potential energy converting and may correspond best with the "baroclinic mode" found by Song (1971, Fig. 5). The $\overline{APE}$ is the same for both prescribed flows used in Fig. 7. Clearly, the short and some middle waves grow much more rapidly in the surface front case. This is not particularly surprising in light of past studies such as Staley and Gall (1977); the shorter wavelength solutions are confined primarily to the lower portion of the fluid and are most responsive to the properties of the basic state there. In the sur-

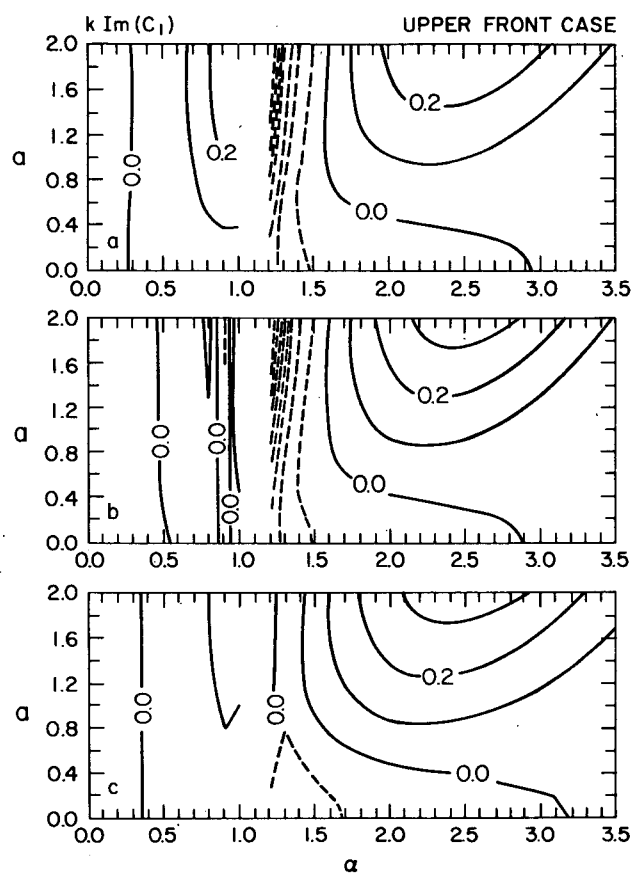

FIG. 6. Second-order growth rate spectra for the cases shown in Fig. 5. The contour interval is 0.1.

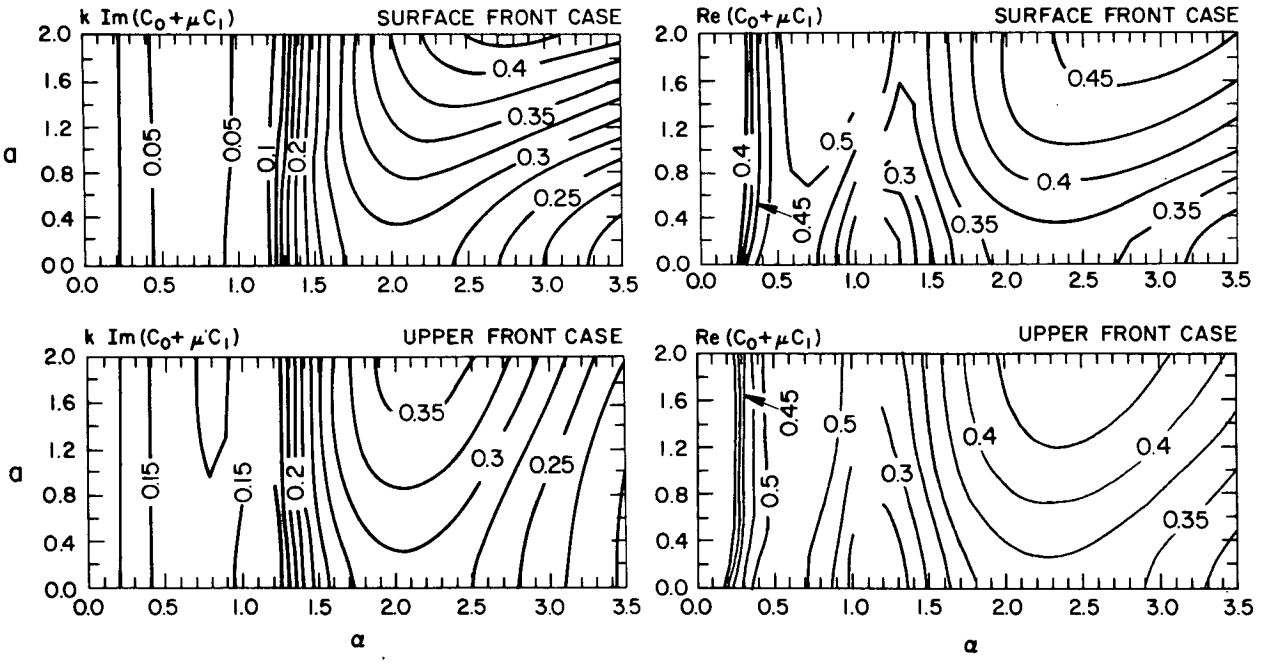

FIG. 7. Total growth rate (upper left) and phase speed spectra (upper right) for the surface front Interface case are shown with the total growth rate (lower left figure) and phase speed spectra (lower right figure) for the upper front Interface case. Values of Λ in Table 1 are used. The contour interval is 0.025.

face front case the $\overline{APE}$ is concentrated near the bottom surface while in the upper front case it is more spread out in the vertical because of the exponential decrease of ρ_s with height. The short waves simply cannot tap this source of energy as efficiently when it is distributed through a large depth as they can when it is highly concentrated at the bottom. The influence of the front is greater in the surface front case and the shorter waves move and grow faster.

Representative intermediate-wavelength cross sections of total pressure amplitude and phase angle (negative values increasing with height imply westward tilt with height) and second-order baroclinic energy conversion for the two Narrow tropopause cases appear in Fig. 8. The properties of the most unstable wave are qualitatively the same as those for $\alpha = 2.0$ shown in Fig. 8. As found by Grotjahn (1979), the amplitude of the eddy is increased in the neighborhood of the front. Again, the tropopause structure influences the upper front solutions more than the surface front results. The differences between cases are generally small for the upper front and insignificant for the surface front for any except the long waves. In the lower portion of the domain the second-order amplitude is slightly larger for the Narrow than for the Broad case; while well above z_T the opposite is true. This tends to compensate the differences found between these two cases at lowest order. The compensation is even more pronounced when the $\overline{APE}$ is the same in both cases. The Interface case is uniformly lower in amplitude for both types of weak front. Other than well above z_T, there is no apparent trend between the three cases for the second-order amplitude (recall that the first-order amplitude did exhibit a clear trend).

The westward tilt with height of the pressure trough and ridge axes was increased in the vicinity of the front. This increase in tilt was slightly stronger in the Narrow tropopause case when Λ was fixed. The phase tilt at these levels was slightly stronger for this case at lowest order as well. If the $\overline{APE}$ is kept constant between the cases, then the tilts are clearly strongest in the Broad case, corresponding with the larger growth rates. In addition, horizontal tilts of the axes indicative of momentum convergence occur generally above the most intense part of the frontal region. Both of these phase modifications were greater for the surface front than upper front even though the $\overline{APE}$ was identical. This means that the barotropic conversion is much weaker for the upper front cases because the convergence occurred at high levels (where ρ_s is small), than for the surface front cases, where the convergence occurred mainly at mid-tropospheric levels. The weak divergence at lower levels is sufficiently strong so that the barotropic conversion is negative, but nearly zero, for the upper front. This conversion is positive for the surface front. In all cases the barotropic conversion is much weaker than the baroclinic.

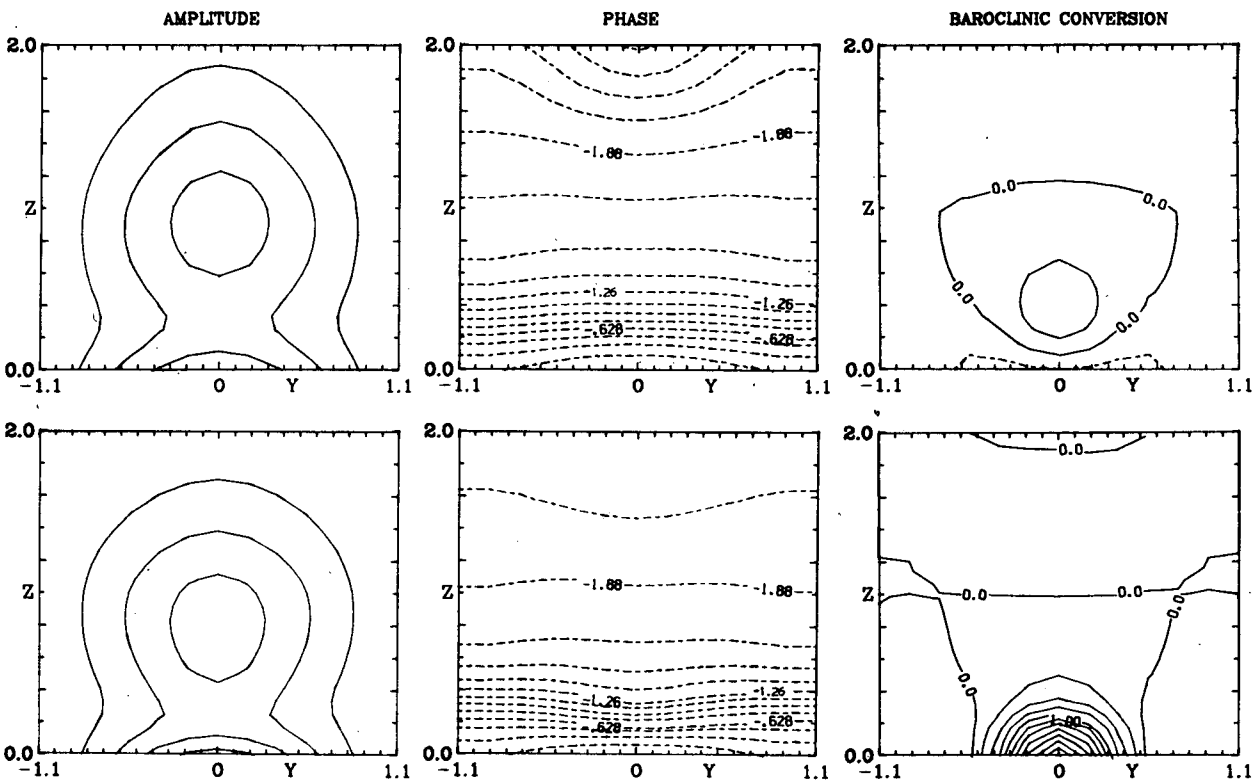

FIG. 8. Meridional cross sections of total pressure amplitude and phase and second-order baroclinic energy conversion for the two Narrow tropopause cases, where $\alpha = 2.0$ and $a = 1.6$. The upper figures are for the upper front case; the lower figures are for the surface front case. Values of Λ in Table 1 are used. The contour intervals are 0.25, $.05\pi$ and 0.25.

The second-order baroclinic energy conversion for the upper front (Fig. 8) reaches a positive maximum at around $z = 0.4$ and is negative along the bottom. There is little difference between the conversions for the various tropopause structures, at least for the faster growing intermediate and short waves. The baroclinic conversion is much larger for the surface front, and is greatest at the bottom. The maximum conversion occurs around the minimum pressure amplitude for the upper front and maximum amplitude of the surface front.

In all cases, the eddy heat flux is poleward over most of the domain, including that above the tropopause. The meridional gradient of basic-state temperature reverses sign above z_T, so the poleward heat flux actually reinforces the basic-state temperature gradient in the lower stratosphere. Thus, these eddies primarily feed on the energy stored as vertical shear of the mean flow in the troposphere. But, since their tropospheric structure persists into the lower stratosphere, they help maintain the height of the jet and reduce the lower stratospheric velocities by increasing the (negative) vertical shear. This conclusion must be tempered with the caveat that these lower stratospheric heat fluxes are small. Even so, similar poleward heat fluxes by transient eddies are commonly observed in the lower stratosphere, though they are greater in amplitude than these results suggest.

The total eddy energy is much larger in the surface front solutions than it is for the upper front. Hence, the wide disparity between the two types of fronts in the energy conversions does not conflict with the smaller differences noted in the growth rates. The ratio of the total energy conversions to total eddy energy can be used to estimate the growth rate. (This estimate includes some higher order contributions.) The estimated growth rates were slightly larger than the calculated growth rates, the differences being largest for the Broad tropopause.

The effects produced by giving the tropopause zone a meridional tilt, higher toward the equator, are now discussed. A tilted Interface case was not examined. The tilt has no effect on the complex phase speed if the meridional range is centered such that $\Delta = 0$ in (11) because the integrals in (9) are antisymmetric and vanish. In the following discussion the meridional range of the tilted tropopause included in $|y| \leq y_b$ is shifted equatorward by an amount Δ.

For $\Delta > 0$ the growth rate and phase speed are both increased (see Fig. 9). The growth rate increases with Δ because the mean height of the tropopause has been lowered thereby increasing the aver-

age vertical shear in the troposphere. Negative values of Δ reduce the growth rate by the converse reason. There is an optimum wavelength ($\alpha \approx 3.0$) for which this meridional shift of the tilted tropopause increases the growth rate most; thus this process also shifts the most unstable wave to shorter wavelengths.

Compared with the complex phase speed, the tilted tropopause causes much larger changes in the eddy amplitude and phase. In the portion of the meridional range where the tropopause generally is below its lowest-order height z_T, the amplitude, westward tilt with height, and consequent local baroclinic energy conversion are all increased. In the range where the tropopause slopes above z_T all three are reduced. These effects are most prominent in the lower part of the domain; around and above z_T the tilt produces very little change. This may explain the greater sensitivity of the short-wave growth rates noted above. Note that U_T has large positive vertical shear in the lower troposphere and smaller negative vertical shear around and above z_T for $y + \Delta > 0$. For $\Delta = 0$ the antisymmetric areas of second-order energy conversion nullify. For $\Delta > 0$ the region of positive conversion slightly exceeds that of negative conversion such that the volume-averaged conversion is small and positive in accordance with the calculated growth rates.

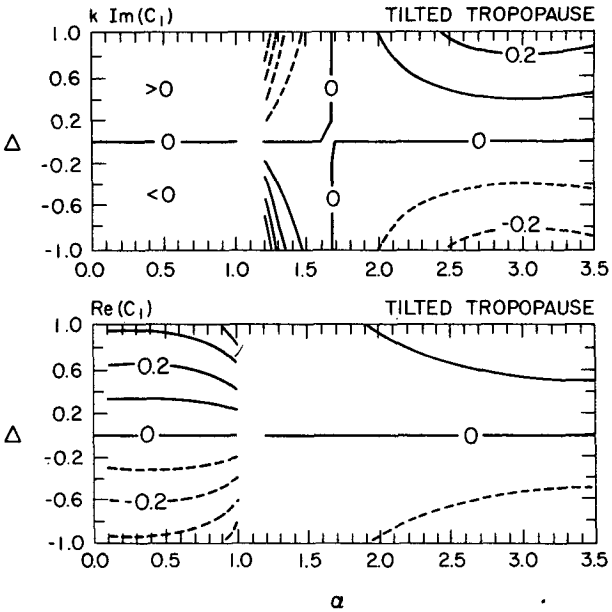

FIG. 9. Second-order growth rate (top) and phase speed (bottom) spectra produced by the tilted tropopause alone. Δ measures the equatorward shift of the tilted tropopause relative to the domain $|y| \leq y_b$. Y = 1.0 and the contour interval is 0.1.

5. Conclusions

This study has sought to investigate the effects of a fixed tropopause zone of variable structure on the stability, structure and energetics of an incipient wave cyclone. The tropopause zone was broad, narrow or infinitesimally thin in the vertical. It could also be tilted in the meridional direction. The linearized tropopause dynamics produced generally small effects; these are discussed in detail in Sections 3 and 4.

The foregoing results are complementary with former studies. The structure of the tropopause produces noteworthy effects on solutions with significant amplitude near the tropopause height z_T. For the lowest-order solutions, narrowing the tropopause zone increases the phase speed, growth rate and upper level relative maximum amplitude of an intermediate wave. These trends are partially compensated by the second-order changes introduced by the upper front when the basic state $\overline{\text{APE}}$ is fixed. When the same velocity profiles (with differing $\overline{\text{APE}}$) are used for the three tropopause structures, these trends are generally magnified. The upper front solutions have greater amplitude at z_T than do the surface front solutions. Thus, the upper front solutions are more greatly modified by various tropopause structures. (Again, true atmospheric fronts are stronger and narrower than the temperature field structure conveniently referred to here as a "front.") Because many of the modifications brought about by varying the thickness of the tropopause zone are small, it is difficult to draw more specific conclusions. Allowing the tropopause zone to have meridional tilt introduces large asymmetries in the solutions. Much of this asymmetry seems associated with the nonuniform distribution of basic current vertical shear that was made in accordance with the tilt. The wave amplitude above z_T is significantly less for the Interface case when the amplitude is decreasing with height at z_T and vice versa. This difference is directly related to the discontinuity of the static stability [through ϵ in (5)] at the interface. The fastest phase speed and growth rate both shift to shorter wavelengths when the meridional width of the frontal zone is smaller. These shifts are greater in the surface front experiments because the short waves are confined primarily near the bottom surface, the same region as the front. The eddy amplitude is increased in the vicinity of the front and the meridional scale of the wave becomes smaller for a narrower prescribed frontal zone. The baroclinic and barotropic energy conversions were much stronger for the surface front than for the upper front cases. With the main exception of the propagation speed spectrum, qualitatively similar conclusions were analyzed in Grotjahn (1979). The differences appear mainly associated with the choice of more reasonable basic currents and upper boundary placement. In this study the influence of the dubious upper boundary is effec-

tively removed by placing it at a much higher altitude than before. The basic current reaches a maximum near the tropopause (see Figs. 1 and 4), whereas before it exponentially increased with height.

This study has shown that the properties of the solution are not extremely sensitive to changes in the linear tropopause structure. In hindsight, this result is not too surprising for two reasons. First, the large changes found in earlier studies occurred when dramatic changes were made where the wave had significant amplitude. Second, the largest changes in this study also occurred when significant changes were made where the forcing function is most important; *viz.*, the top and bottom boundary conditions and the presence or absence of interface conditions. The interior forcing function for this problem is not the major factor and its influence on the solutions is relatively minor. The changes between the Broad and Narrow cases principally affected the interior forcing function and had little effect on the boundary forcing. Clearly, this influence is also small at lowest order, where the problem is homogeneous. Thus, the differences between the two cases are not large. If there are to be dramatic changes, it is anticipated that these will occur through nonlinear interaction between the cyclone and tropopause. From the arguments above, it is anticipated that the greatest effects will arise for the Interface case when the interface is allowed to be deformed by the eddy. These conclusions will form the foundation for my future study of tropopause dynamics.

Acknowledgments. I thank Drs. R. Sweet, P. Swarztrauber, J. Tribbia and C. Leith for their assistance and comments regarding this research. I thank V. Leeburg and U. Rosner for typing this manuscript.

APPENDIX

Symbols List

$\overline{\text{APE}}$ zonal mean available potential energy

$$\left[= \int_0^{z\ \text{TOP}} \tfrac{1}{2}\epsilon\rho_s(U_z)^2 dz \right]$$

B_i vertical boundary equations forcing function at order μ^i

C complex phase speed $[=C_0 + \mu C_1 + \cdots]$

D vertical length scale (=10 km)

F_i interior equations forcing function at order μ^i

f, f_0 variable, constant mean Coriolis parameter

g acceleration of gravity

k zonal wavenumber

L Rossby radius of deformation at surface: horizontal length scale (≈1100 km)

U basic-state zonal wind $[= -\psi_y]$

U_T tilted tropopause $O(\mu)$ part of U

V horizontal length scale

x zonal coordinate

y meridional coordinate

z vertical coordinate

z_T mid-height of tropopause zone (=10 km)

α $[=k\sqrt{2}]$

β first meridional derivative of f

Δ tilted tropopause meridional shift

ϵ $[=f_0^2L^2/g\kappa D]$

θ_s horizontal mean potential temperature

κ static stability $[=D(\ln\theta_s)_z]$

Λ $O(\mu)$ $\overline{\text{APE}}$ normalizer

λ parameter in ϵ expression (4b)

ξ transform coordinate $[=1 - \exp(-z)]$

μ Rossby number $[=V/f_0L = 0.2]$

ρ_s horizontal mean density profile

Υ amount of tilt parameter [see (11)]

ϕ eddy pressure $[=\mu\phi_0 + \mu^2\phi_1 + \cdots]$

ψ basic-state pressure $[=\psi_0 + \mu\psi_1]$

Ω $[=(\ln\rho_s)_z]$

REFERENCES

Árnason, G., P. S. Brown and E. A. Newburg, 1967: A case study of the validity of finite difference approximations in solving dynamic stability problems. *J. Atmos. Sci.*, **24**, 10–17.

Bleck, R., 1979: A sensitivity study concerning vertical resolution in atmospheric prediction models. *Preprints Fourth Conf. Numerical Weather Prediction*, Silver Spring, Amer. Meteor. Soc., 161–164.

Blumen, W., 1979: On short-wave baroclinic instability. *J. Atmos. Sci.*, **36**, 1925–1933.

Brown, J. A., 1969: A numerical investigation of hydrodynamic instability and energy conversions in the quasi-geostrophic atmosphere: Part I. *J. Atmos. Sci.*, **26**, 352–365.

Charney, J. G., and P. G. Drazin, 1961: Propagation of planetary-scale disturbances from the lower into the upper atmosphere. *J. Geophys. Res.*, **66**, 83–109.

Duncan, C. N., 1977: A numerical investigation of polar lows. *Quart. J. Roy. Meteor. Soc.*, **103**, 255–267.

Gill, A. E., J. S. A. Green and A. J. Simmons, 1974: Energy partition in the large-scale ocean circulation and the production of mid-ocean eddies. *Deep-Sea Res.*, **21**, 499–528.

Green, J. S. A., 1960: A problem in baroclinic stability. *Quart. J. Roy. Meteor. Soc.*, **86**, 237–251.

Grotjahn, R., 1979: Cyclone development along weak thermal fronts. *J. Atmos. Sci.*, **36**, 2049–2074.

——, 1981: Stability properties of an arbitrarily oriented mean flow. *Tellus* (in press).

Moen, L., 1974: A spectral model for investigation of amplifying baroclinic waves. *Tellus*, **26**, 424–443.

Simmons, A. J., and B. J. Hoskins, 1977: Baroclinic instability on the sphere: Solutions with a more realistic tropopause. *J. Atmos. Sci.*, **34**, 581–588.

Song, R. T., 1971: A numerical study of the three-dimensional structure and energetics of unstable disturbances in zonal currents: Part II. *J. Atmos. Sci.*, **28**, 565–586.

Staley, D. O., and R. L. Gall, 1977: On the wavelength of maximum baroclinic instability. *J. Atmos. Sci.*, **34**, 1679–1688.